OATAO

Open Archive Toulouse Archive Ouverte

Open Archive Toulouse Archive Ouverte (OATAO)

OATAO is an open access repository that collects the work of Toulouse researchers and makes it freely available over the web where possible.

Structure and electrical properties of single-phase cobalt manganese oxide spinels $Mn_{3-x}Co_xO_4$ sintered classically and by spark plasma sintering (SPS)

Hélène Bordeneuve [a,*], Sophie Guillemet-Fritsch [a], Abel Rousset [a],
Sophie Schuurman [b], Véronique Poulain [b]

[a] Centre Interuniversitaire de Recherche et d'Ingénierie des Matériaux (CIRIMAT), UMR-CNRS 5085, Université Paul Sabatier, Bât 2R1, 118 Route de Narbonne, 31 062 Toulouse Cédex 4, France
[b] Vishay-BC Components, Avenue F. Guillaumelaan 70, B-1140 Bruxelles, Belgium

Corresponding author. Fax: +33 5 61 55 61 63.
E-mail address: bordeneuve@chimie.ups-tlse.fr (H. Bordeneuve).

ABSTRACT

Cobalt manganese oxide spinels $Mn_{3-x}Co_xO_4$ (with $0.98 \leqslant x \leqslant 3$) were prepared by the thermal decomposition in air of oxalate precursors. The influence of the thermal treatments on the structure of these materials is emphasized. Single-phase ceramics were obtained after optimization of the sintering parameters. A precise phase diagram for the Co–Mn–O system is proposed according to thermal stability and structure of oxide powders. The electrical measurements on single-phase ceramics show that low values of resistivity can be achieved. The conduction could take place through jumps of polarons between Mn^{3+} and Mn^{4+} on octahedral sites. These compounds present interesting electrical characteristics for negative temperature coefficient (NTC) thermistor applications.

Keywords:
Cobalt manganese oxide
Spinels
SPS sintering
Thermal history
Electrical properties
Thermistors

1. Introduction

The study of cobalt manganese oxide spinels is made complex by the multiple oxidation states of manganese and cobalt and different structural possibilities. Thus, even for the compound $MnCo_2O_4$, several cationic distributions have been proposed [1–9] following the use of different characterization techniques (Table 1). The oxygen content and the distribution of the cations on the different crystallographic sites are sensitive to the sample preparation methods, which makes the prediction of the cationic distribution difficult. In this study, the oxide powders were prepared via the oxalate precursor route. The structural evolution and the thermal stability were determined as a function of temperature.

The main studies reported on cobalt manganese oxides have principally concerned powders or thin films [10–13]. Although there have been some works on ceramics [1,2,14], no results have been published on detailed preparation conditions and particularly, on the difficulty to obtain the single-phase over the whole composition range $0.98 \leqslant x \leqslant 3$. Precise control of the manufacturing parameters is needed, so the sintering temperature, the cooling rate and the sintering method have to be adapted for each composition.

These Mn-based spinels are oxide semiconductors. Unlike for Mn–Ni–O and Mn–Ni–Co–O systems that are largely used as negative temperature coefficient (NTC) thermistors [15,16], data on electrical properties are still lacking. To our knowledge, the only works reported for Mn–Co–O systems were those done by Kolomiets [1] and Jabry [8] on ceramics with low densification and/or multiple phases. The evolution of resistivity values with the composition is of primary interest for potential applications as NTC thermistors, and will provide information together with the structure, on the cation distribution.

In this paper, we focused on the preparation of bulk single-phase ceramics over the composition domain $0.98 \leqslant x \leqslant 3$ and the determination of their electrical properties.

2. Experimental

2.1. Sample preparation

Cobalt manganese oxalic precursors, $Mn_{1-\alpha}Co_\alpha C_2O_4 \cdot nH_2O$, were obtained by the co-precipitation of an aqueous solution of ammonium oxalate (concentration 0.2 mol/L) and a mixture of manganese and cobalt nitrates, in the desired proportions
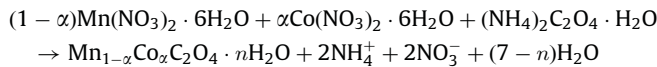
Table 1
Cationic distributions of defined MnCo$_2$O$_4$ proposed in the literature.

References	Year	Technique employed	Cationic distributions
Kolomiets et al. [1]	1957	Electrical conductivity	$Co^{2+}[Co^{2+}Mn^{4+}]O_4^{2-}$
Wickham and Croft [2]	1958	X-ray diffraction, magnetism	$Co_x^{2+}Mn_{1-x}^{2+}[Mn_2^{3+}]O_4^{2-}$ for $0<x<1$
			$Co_{x-1}^{2+}[Co_{x-1}^{3+}Mn_{3-x}^{3+}]O_4^{2-}$ for $1.8<x<3$
Aoki [3]	1961	X-ray diffraction, electrical conductivity, thermogravimetric analyses	$Mn_{0.04}^{2+}Co_{0.96}^{2+}[Co_{0.04}^{2+}Co^{3+}Mn_{0.96}^{3+}]O_4^{2-}$
Blasse [4]	1963	Magnetism	$Co^{2+}[Co^{2+}Mn^{4+}]O_4^{2-}$
Boucher et al. [5]	1970	Neutron diffraction and magnetism	$Co^{2+}[Co^{3+}Mn^{3+}]O_4^{2-}$
Gautier et al. [6]	1982	X-ray diffraction, magnetism	$Co^{2+}[Co^{3+}Mn_{0.35}^{2+}Mn_{0.29}^{3+}Mn_{0.36}^{4+}]O_4^{2-}$
Yamamoto et al. [7]	1983	Neutron diffraction	$Mn_{0.25}Co_{0.75}[Mn_{0.75}Co_{1.25}]O_4$
Jabry et al. [8]	1988	X-ray diffraction, electrical conductivity	$Co^{2+}[Mn_{2-2u}^{3+}Mn_u^{4+}Co_u^{2+}]O_4^{2-}$ with $u=x-1$ for $1<x<2$
			$Co^{2+}[Mn_{1-v}^{4+}Co_{1-v}^{2+}Co_{2v}^{3+}]O_4^{2-}$ with $v=x-2$ for $2<x<3$
Rios et al. [9]	1998	X-ray diffraction, magnetism, electrochemical measurements	$Co^{2+}[Co^{III}Mn_{0.45}^{3+}Mn_{0.55}^{4+}]O_4(OH)_{8.55}$ Co^{III}: low spin

Table 2
Composition of the synthesized cobalt manganese oxalates $Mn_{1-\alpha}Co_\alpha C_2O_4 \cdot nH_2O$ and the corresponding oxides $Mn_{3-x}Co_xO_4$ ($x=3\alpha$).

α	0.33	0.42	0.51	0.59	0.66	0.74	0.79	0.87	0.92	0.98	1
x	0.98	1.27	1.54	1.78	1.99	2.22	2.39	2.60	2.77	2.93	3

(concentration 4 mol/L). After 30 min of ageing, the solution was filtered, washed several times with water and dried at 90 °C in air. The synthesis reaction can be summarised as

$$(1-\alpha)Mn(NO_3)_2 \cdot 6H_2O + \alpha Co(NO_3)_2 \cdot 6H_2O + (NH_4)_2C_2O_4 \cdot H_2O$$
$$\rightarrow Mn_{1-\alpha}Co_\alpha C_2O_4 \cdot nH_2O + 2NH_4^+ + 2NO_3^- + (7-n)H_2O$$

These precursors were then heated in air at 800 °C. The resulting oxide powders were mixed with an organic binder and pressed at 500 MPa into 6 mm discs. The discs were then sintered using the conventional process at different temperatures 1100 °C $\leqslant T \leqslant$ 1280 °C in air and cooled at different rates, depending on the composition. The various cooling rates were chosen in order to show the influence of the process parameters on the structure and the electrical properties of ceramics. A more recent technique, spark plasma sintering (SPS) was also used to sinter the ceramics. In this case, the powder was introduced in an 8 mm internal diameter graphite matrix die which was previously lined with 0.75 mm thick graphitized paper and pre-compacted. In the SPS device, the temperature was measured using a thermocouple focused on the graphite matrix. The powders were sintered under vacuum between 700 and 750 °C, according to the composition of samples, with an applied load of 50 MPa using a Sumitomo 2080 apparatus. (PNF2 CNRS platform available at the University of Toulouse, France).

2.2. Sample characterization

Table 2 presents the chemical composition of the powders determined in the solid state (calcined powders) by plasma emission spectroscopy with a Jobin Yvon 2000 apparatus. To identify the phases and to measure the lattice constants, all samples were analyzed by X-ray diffraction (XRD) using a Bruker D4 Endeavor X-ray diffractometer. XRD patterns were refined by the Rietveld method associated with the Fullprof/WinplotR software package. High temperature XRD studies were carried out using an MRI chamber mounted on a Bruker D8 diffractometer. For each composition, oxide powders were heated to 60 °C/min up to 1000 °C. Thermogravimetric analyses of the oxide powders were performed on a Setaram TAG 16 apparatus. The samples

were submitted to a heating cycle from room temperature to 1300 °C at a 3 °C/min heating rate. The bulk density was determined from the mass/volume ratio for the fired ceramics. In order to measure electrical resistivity of the ceramics, their faces were covered by evaporation with a thin film of gold of about 100 nm thickness. Resistance measurements were taken in an oil bath between 25 and 150 °C by a two-probe technique using a Philips PM 2525 multimeter.

3. Results and discussion

3.1. Structure and thermal stability of powders $Mn_{3-x}Co_xO_4$ ($0.98 \leqslant x \leqslant 3$)

As mentioned in the introduction, only few studies exist on ceramics. In order to understand the behavior of ceramics, the structure and the thermal stability of oxide powders were first examined.

The oxide powders $Mn_{3-x}Co_xO_4$ ($0.98 \leqslant x \leqslant 3$) were obtained after heat treatment in air at 800 °C for 4 h and a cooling rate of 150 °C/h. The structure strongly depends on the chemical composition.

For $0.98 \leqslant x \leqslant 1.54$, X-ray diffraction measurements show that the oxides consisted of a mixture of tetragonal I4$_1$/amd and cubic Fd3m spinel-type phases at room temperature (Fig. 1). Quantitative phase analyses have been undertaken with the Rietveld method. Since cobalt and manganese cannot be distinguished with X-rays, the refinements have been made with 50% of cobalt and manganese on each crystallographic site. The tetragonal phase was the main phase present for $x=0.98$ (92%), and decreased with the cobalt content. It became minor for $x=1.54$ (34%), the main phase being the cubic one. The tetragonal distortion from cubic symmetry is due to the high Mn^{3+} ion content at octahedral sites ($>60\%$; cooperative Jahn–Teller effect).

For $x \geqslant 1.78$, the oxides crystallize in the cubic Fd3m spinel-type structure. The compositional limit of the cubic cobalt manganese spinel phase strongly depends on the synthesis procedure and on the thermal history and varies between $x=1.6$ [17] and 1.8 [2].

Then, the behavior of oxide powders $Mn_{3-x}Co_xO_4$ ($0.98 \leqslant x \leqslant 3$) with temperature was followed by thermal analysis. TGA curves for three compositions ($x=1.54$, 1.99 and 3) are shown in Fig. 2. They were heated from room temperature up to 1300 °C under a flow of air.
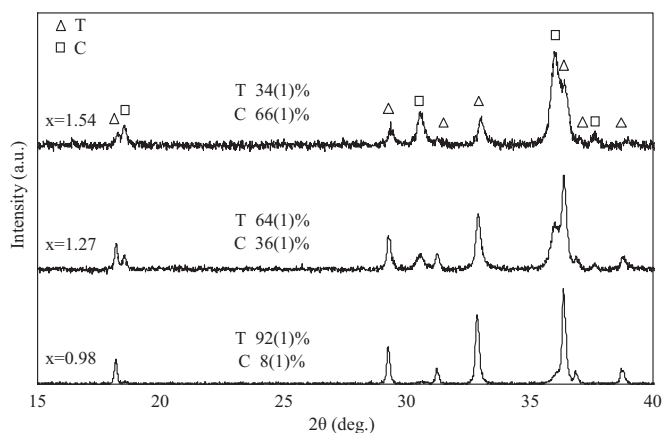
For Co$_3$O$_4$ (cationic distribution Co^{2+}[Co^{3+}]$_2$O$_4$ [18]), the mass loss around 913 °C was assigned to the reduction of Co^{3+} on

octahedral sites according to the reaction

$$Co_3O_4 \rightarrow 3CoO + \tfrac{1}{2}O_2 \ [19]$$

For spinel oxides with $x<3$, the temperature of reduction increases due to a decreasing amount of Co^{3+}. During cooling, the mass gain corresponds to a progressive reoxidation. This reoxidation is complete only for Mn-rich samples but becomes increasingly difficult as the cobalt content increases. For higher cobalt contents, after thermal analysis, the spinel is no longer the unique phase. Slow cooling led to more reoxidation and less impurity phase. The temperatures of reduction were determined on our samples for $0.98 \leqslant x \leqslant 3$ and added to the phase diagram reported by Aukrust and Muan [20] (Fig. 3). They are in agreement with their results.

Moreover, the structural transformations with temperature were followed by high temperature X-ray diffraction until 1000 °C. For $0.98 \leqslant x \leqslant 1.54$, the tetragonal spinel phase decreases with temperature. It disappears at high temperature and a single cubic spinel phase is observed. An example is given for $x = 0.98$ in Fig. 4 with transition at 900 °C. Tetragonal–cubic transition with temperature has already been reported for spinels with the formula MMn_2O_4 (where $M = Mn$, Mg, Zn, Cd, Co and Fe) [21,22]. For $x \geqslant 1.78$, no structural transformations take place but for higher cobalt contents the presence of the additional phase (Mn,Co)O to the spinel (due to the reduction) is observed and confirms that deduced from the thermal analyses.
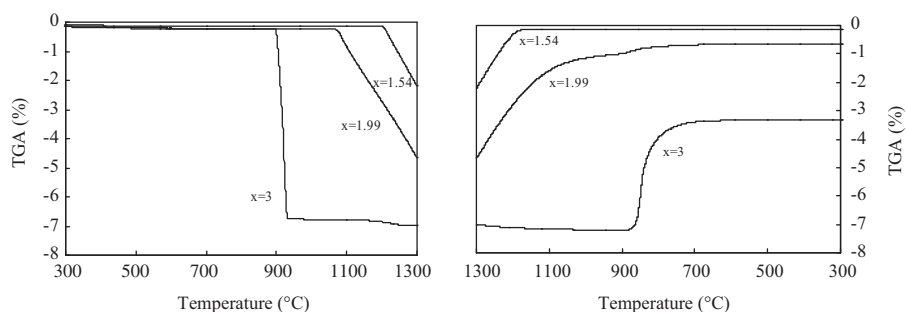
3.2. Influence of the sintering process (temperature and cooling rate) on the structure of cobalt manganese oxide ceramics

In order to study the influence of the sintering process on the structure of cobalt manganese oxide ceramics, different temperatures, dwell times and cooling rates were chosen. In all cases, for conventional sintering, a heating rate of 40 °C/h up to 450 °C was used in order to slowly eliminate the organic binder, and was then increased to 80 °C/h up to the sintering temperature. The results are presented in to two composition domains, because:

- for Mn-rich oxides ($0.98 \leqslant x \leqslant 1.54$), the preparation of single-phase ceramics is limited by numerous structural transformations occurring at various temperatures;
- for Co-rich oxides, the difficulty comes from the reduction of the cubic spinel phase at low temperatures.

The process conditions for conventional sintering in air for the oxides in the composition range $0.98 \leqslant x \leqslant 1.54$ and the corresponding structure of the ceramics are reported in Table 3. A quench in air performed from high temperature in the single cubic spinel phase domain, allowed single phase ceramics to be obtained. Instead of the cubic spinel phase observed at high temperature in the X-ray diagrams, quenched ceramics are tetragonally distorted. Indeed, the cubic phase is thermodynamically stable only at high temperature and cannot be isolated at room temperature [14,17]. For $x = 0.98$ and 1.27, dense pellets could not be obtained without cracks. These cracks originate from the thermal shock leading to a rapid cubic-to-tetragonal phase transition. As a consequence, samples were also quenched at lower temperatures but still in the single phase domain (900 °C for $x = 0.98$ and 800 °C for $x = 1.27$); the cracks were limited for $x = 0.98$ and disappeared for $x = 1.27$. When the quenching temperature was lowered again, two tetragonal spinel phases appeared: one being the tetragonal phase of the starting oxide powder and the other coming from the cubic high temperature spinel after the quench [17]. When the cooling rate was lowered to 200 °C/h, the cubic high temperature single phase decomposed into a mixture of cubic and tetragonal spinel phases.

For $1.78 \leqslant x \leqslant 2.22$, the process conditions for conventional sintering in air and the corresponding structure of ceramics are reported in Table 4. In this composition range, the reduction of the spinel phase appeared at relatively low temperature (from 1150 °C for $x = 1.78$ to 900 °C for $x = 3$) and prevented the formation of well-dense single-phase ceramics. For $x = 1.78$, a cooling rate of 30 °C/h led to ceramics presenting three different phases: tetragonal and cubic spinel phases and CoO. When the cooling rate was sufficiently low, the ceramic reoxidized again into the single phase. However, as the cobalt content increased, the

Fig. 1. X-ray diffraction pattern of the oxide powders $Mn_{3-x}Co_xO_4$ with $x = 0.98$; 1.27; 1.54 (T: tetragonal spinel phase; C: cubic spinel phase).

Fig. 2. TGA curves recorded on oxide powders with $Mn_{3-x}Co_xO_4$ with $x = 1.54$; 1.99; 3. For the sake of clarity, only three compositions are presented: (a) heating from 25 to 1300 °C and (b) cooling from 1300 to 25 °C.
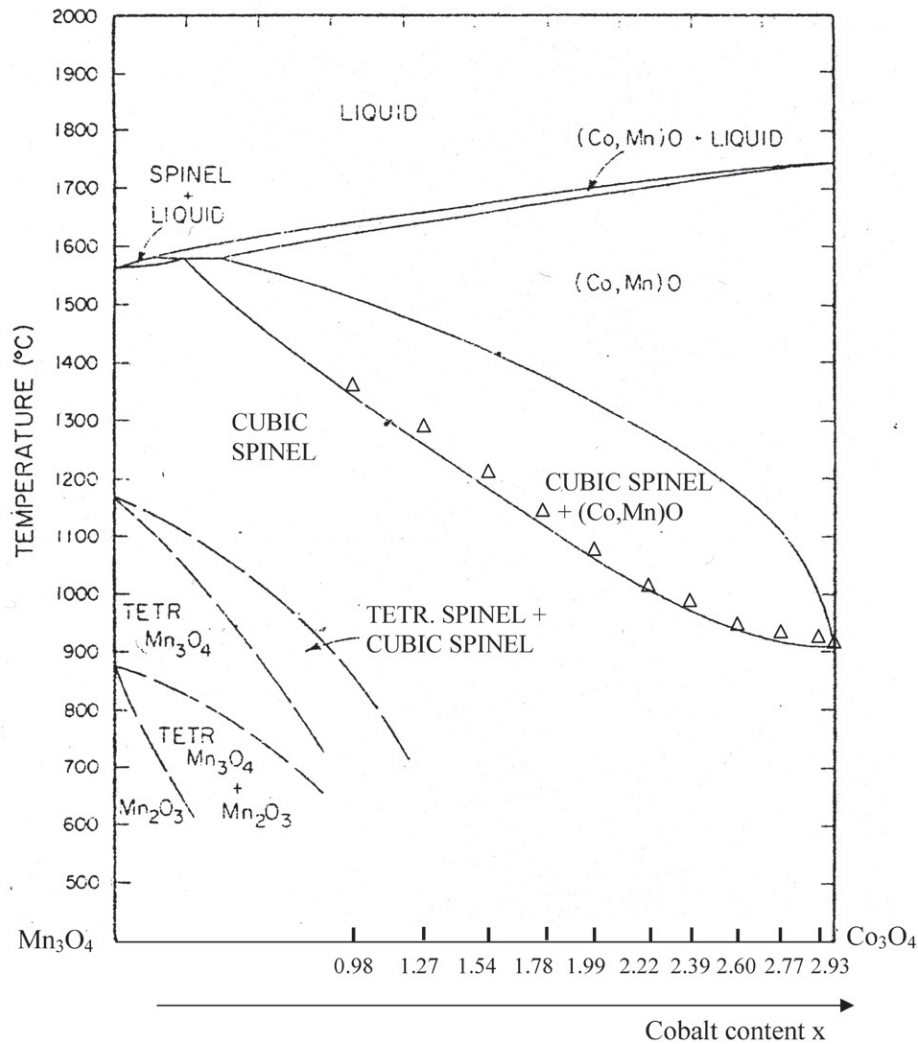
Fig. 3. Diagram showing phase relations in the system cobalt oxide-manganese oxide in air as reported by Aukrust and Muan [20] (Δ points obtained in the present study by thermal analysis).

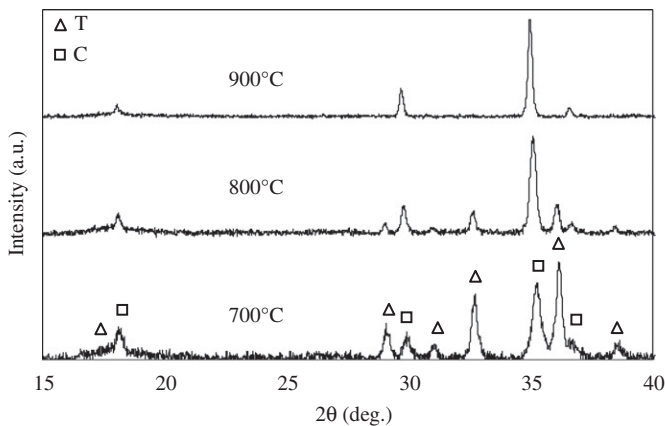**Fig. 4.** X-ray diffraction pattern of the oxide powder $Mn_{2.02}Co_{0.98}O_4$ (*T*: tetragonal spinel phase; *C*: cubic spinel phase).

kinetics of reoxidation during cooling became really slow. This is the reason why dense single-phase ceramics were not obtained by "conventional sintering" for $x > 1.78$. As a consequence, another sintering technique called SPS was used for these particular samples. It allowed a significant decrease of the sintering temperature (700 °C, which is lower than the lowest reductive temperatures) while reaching high densities (Table 5). We first checked the similarity of the structure for ceramics of the same composition ($x = 1.78$) and sintered by the two different methods. The experiments were then done on samples with $x \geqslant 1.99$. Due to the reductive atmosphere in the apparatus, the rock salt ($Mn_{1-x/3}Co_{x/3}$)O appears on the surface of the ceramics. But after polishing the surface, cubic spinel single-phase ceramics with $x \geqslant 1.99$ and of high density were obtained for the first time, by SPS. energy dispersive analysis (EDS) performed on the ceramic fractures showed that the Mn/Co content is the same as in oxide powders.

So, obtaining single phase ceramics implies an adjustment of the process parameters for each composition.

The experimental values of lattice parameters $a' = a\sqrt{2}$, c and the distorsion parameter c/a' were determined for single spinel phase ceramics, whatever the sintering method. They are plotted as a function of composition in Fig. 5. For $0.98 \leqslant x \leqslant 1.54$, as the cobalt content increases, the c/a' ratio decreases, indicating a decrease of Mn^{3+} concentration on octahedral sites. For $1.78 \leqslant x \leqslant 3$, the lattice parameter decreased from 0.832 nm for $x = 1.78 - 0.808$ nm for $x = 3$. The linear decrease of the lattice parameter versus cobalt content confirms Vegard's law. As a first

Table 3
Structural evolution of Mn$_{3-x}$Co$_x$O$_4$ ceramics as a function of the temperature, the dwell time and the cooling rate for $0.98 \leqslant x_{Co} \leqslant 1.54$ (T: tetragonal spinel phase; C: cubic spinel phase).

x	0.98			1.27			1.54		
Structure of oxide powders	C+T			C+T			C+T		
Sintering T (°C)	1280			1180			1180		
Dwell time (h)	8			8			8		
Cooling rate	120 °C/h; quench at 900 °C	120 °C/h; quench at 750 °C	200 °C/h	120 °C/h; quench at 800 °C	120 °C/h; quench at 650 °C	200 °C/h	Quench	120 °C/h	30 °C/h
Structure of ceramics	T	T1+T2	C+T	T	T1+T2	C+T	T	C^a+T	C^a+T
Densification (%)	94			93			93	93	94

^{a} Trace (<2%).

Table 4
Structural evolution of Mn$_{3-x}$Co$_x$O$_4$ ceramics as a function of the temperature, the dwell time and the cooling rate for $1.78 \leqslant x_{Co} \leqslant 2.22$.

x	1.78		1.99	2.22	
Sintering T (°C)	1160		1160	1100	
Dwell time (h)	8	2	2	1	
Cooling rate	30 °C/h	10 °C/h until 400 °C; 20 °C/h until 25 °C	3 °C/h until 500 °C; 30 °C/h until 25 °C	8 °C/h	3 °C/h until 500 °C; 30 °C/h until 500 °C
Structure	C+T+CoO	C	C+CoO	C+CoO	C+CoO
Densification (%)		94			

T: tetragonal spinel phase; C: cubic spinel phase.

Table 5
Structural evolution of Mn$_{3-x}$Co$_x$O$_4$ ceramics sintered by the SPS technique as a function of the temperature, the dwell time and the cooling rate for $1.78 \leqslant x \leqslant 3$ (C: cubic spinel phase).

x	1.78	1.99	2.22	2.39	2.60	2.77	2.93	3
Sintering T (°C)		750				700		
Dwell time (min)				5				
Cooling rate				Power shut off				
Structure before polishing				C+(Mn,Co)O				
Structure after polishing				C				
Densification (%)	95	95	97	97	97	96	96	92
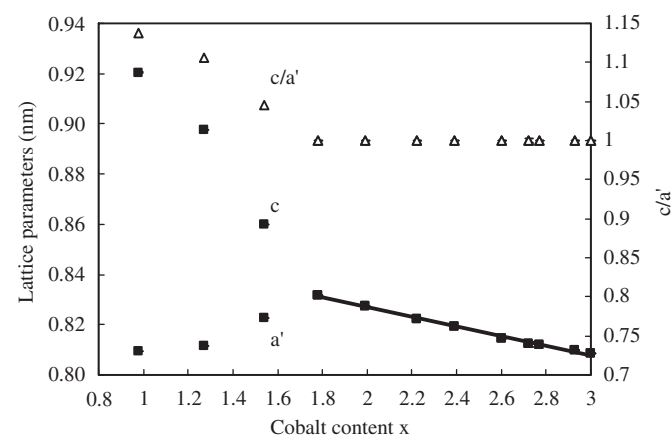
Fig. 5. Lattice parameters versus cobalt content for single phase ceramics ($0.98 \leqslant x \leqslant 3$).

approximation, it is highly probable that the Mn^{3+} ions are substituted for Co^{3+} on the octahedral sites. The Co^{3+} ions (low spin) have a smaller ionic radius than Mn^{3+} ions (high spin) ($r_{Co}^{3+} = 0.0545$ nm and $r_{Mn}^{3+} = 0.0645$ nm) [23]. This hypothesis is confirmed by the oxygen–cation distance on the octahedral sites, that is smaller for Co^{3+} than for Mn^{3+} ($d_{Co}^{3+} = 0.1892$ nm and

$d_{Mn}^{3+} = 0.2045$ nm) [24,25]. These lattice parameters are in agreement with those of the oxide powders.

3.3. Electrical properties of cobalt manganese oxide ceramics

We first checked that the electrical properties of ceramics of fixed composition ($x = 1.78$) sintered with two different methods (classic and SPS) were similar ($\rho = 387 \, \Omega$ cm for the classic method and 380 Ω cm for the SPS). Thus, the electrical properties of single phase ceramics were investigated over the whole composition domain, for all sintering methods.

The resistivity was determined, at 25 °C, for ceramics of each composition sintered using the standard technique and those sintered by SPS. This is presented in Fig. 6 for $0.98 \leqslant x < 3$, because of the poor reproducibility for samples with $x = 3$. Contrary to Mn$_3$O$_4$ (cationic distribution Mn^{2+}[Mn^{3+}]$_2$O$_4$ [26]) and Co$_3$O$_4$ (cationic distribution Co^{2+}[Co^{3+}]$_2$O$_4$ [18]) that are insulators [27,28], the compounds Mn$_{3-x}$Co$_x$O$_4$ ($0.98 \leqslant x \leqslant 2.93$) are semiconductors. The resistivity sharply decreases with the cobalt content down to a minimum of $x = 1.78$ (corresponding to the tetragonal–cubic transition). For higher cobalt contents, it changes less drastically. The resistivity values (ρ varying from 387 Ω cm for $x = 1.78$–49552 Ω cm for $x = 0.98$) are comparable to that of Jabry [8].

As an example, the resistivity of the ceramic Mn$_{1.01}$Co$_{1.99}$O$_4$ was determined as a function of temperature. It decreased
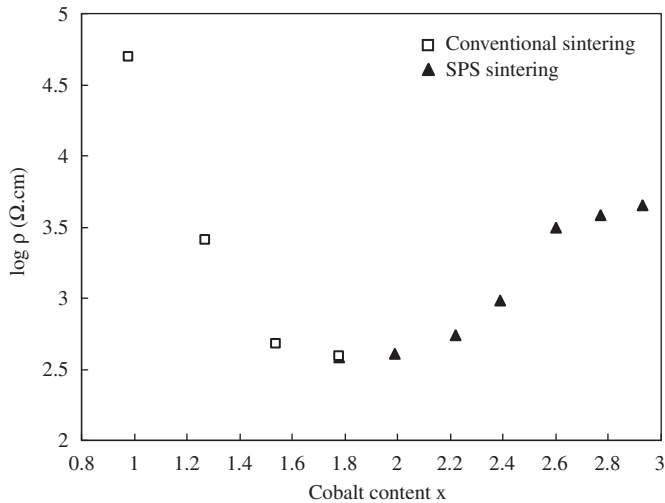
Fig. 6. Log ρ versus cobalt content ($0.98 \leqslant x \leqslant 3$).
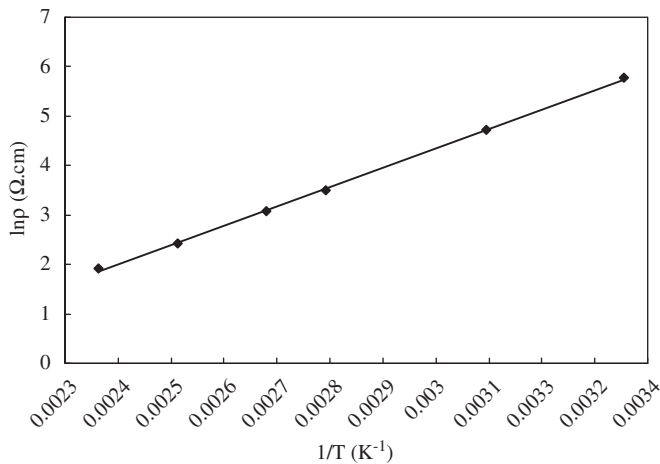

Fig. 7. Ln ρ versus the reciprocal of the temperature between 25 and 150 °C.

exponentially as the temperature increased. The logarithm of ρ as a function of $1/T$ is linear (Fig. 7), which is characteristic of the conduction process described by an Arrhenius law (1):

$$\rho = \rho_0 \, \exp(E_a/kT) \tag{1}$$

This result indicates that cobalt manganese oxides have "thermistor" characteristics. Moreover, their low resistivity is of particular interest for NTC applications.

The mechanism of electrical conduction for the spinel oxides has been described by Verwey [29], through the appearance in the octahedral sites of the spinel lattice, of two types of ions of the same metal, but at different valencies, the electrical conduction taking place by polarons jumps between neighboring ions which thus change their valency. As proposed in the spinel systems Mn–Ni–O, Mn–Ni–Co–O, Mn–Cu–O,… the process probably occurs via Mn^{3+} and Mn^{4+} on octahedral sites [30–32]. This hypothesis is in agreement with cationic distributions given by Rios et al. [9] and Jabry [8].

4. Conclusion

Cobalt–manganese oxides $Mn_{3-x}Co_xO_4$ solid solutions ($0.98 \leqslant x \leqslant 3$) were prepared from mixed oxalic precursors and heat treatment at 800 °C. For $0.98 \leqslant x \leqslant 1.54$, X-ray diffraction

analysis showed a mixture of tetragonal and cubic spinel phases. For $x \geqslant 1.78$, oxides crystallized in a single cubic spinel phase. Thermal treatments had a direct influence on the structure of these materials. For each composition, the sintering parameters had to be adapted to obtain dense single phase ceramics. Two composition domains can be isolated: for $0.98 \leqslant x \leqslant 1.54$, structural transformations with temperature involve quenching at high temperature ($\geqslant 900$ °C); for $1.78 \leqslant x \leqslant 3$, a reduction of the cubic spinel phase between 900 and 1150 °C required slow cooling to allow oxygen to be taken up. But, as the cobalt content increased, the reaction became less reversible. That is the reason why, for $x \geqslant 1.99$, it was interesting to use the SPS technique to obtain single phase ceramics. This innovative technique is an alternative to standard sintering processes and was successfully used here for the first time on this type of materials. Then, the electrical properties of the single-phase ceramics were determined over the whole composition range, whatever the sintering method. Minimum resistivity was obtained for $x = 1.78$. Conduction takes place by a hopping of polarons via cations Mn^{3+} and Mn^{4+} located on octahedral sites. These electro-ceramics should find interesting industrial applications as NTC thermistors.

References

[1] B.T. Kolomiets, J. Sheftel, E. Kurlina, Sov. Phys. Tech. Phys. 2 (1957) 40–58.
[2] D.G. Wickham, W.J. Croft, J. Phys. Chem. Solids 7 (1958) 351–360.
[3] I. Aoki, Jpn. J. Appl. Phys. 17 (1962) 53–61.
[4] G. Blasse, Philips Res. Rep. 18 (1963) 383–392.
[5] B. Boucher, R. Buhl, R. Di Bella, M. Perrin, J. Phys. 31 (1970) 113–119.
[6] J.L. Gautier, S. Barbato, J. Brenet, C.R. Acad. Sci. Paris 294 (1982) 427–430.
[7] N. Yamamoto, S. Higashi, S. Kawano, N. Achiwa, J. Mater. Sci. Lett. 2 (1983) 525–526.
[8] E.H. Jabry, A. Rousset, A. Lagrange, Phase Transform. 13 (1988) 63–71.
[9] E. Rios, J.L. Gautier, G. Poillerat, P. Chartier, Electrochim. Acta 44 (1998) 1491–1497.
[10] F.M.M. Borges, D.M.A. Melo, M.S.A. Câmara, A.E. Martinelli, J.M. Soares, J.H. de Araujo, F.A.O. Cabral, J. Magn. Magn. Mater. 302 (2006) 273–277.
[11] G.P. Vasil'ev, L.A. Pakhomov, L.A. Ryabova, Thin Solid Films 66 (1980) 119–124.
[12] E. Rios, G. Poillerat, J.F. Koenig, J.L. Gautier, P. Chartier, Thin Solid Films 264 (1995) 18–24.
[13] J.L. Martin de Vidales, E. Vila, R.M. Rojas, O. Garcia-Martinez, Chem. Mater. 7 (1995) 1716–1721.
[14] R. Buhl, J. Phys. Chem. Solids 30 (1969) 805–812.
[15] A. Feltz, J. Topfer, F. Schirrmeister, J. Eur. Ceram. Soc. 9 (1992) 187–191.
[16] T. Yokoyama, T. Meguro, S. Okazaki, H. Fujikawa, T. Ishikawa, J. Tatami, T. Wakihara, K. Komeya, T. Sasamoto, Adv. Mater. Res. 29–30 (2007) 359–362.
[17] E. Vila, R.M. Rojas, J.L. Martin de Vidales, O. Garcia-Martinez, Chem. Mater. 8 (1996) 1078–1083.
[18] E.W. Gorter, Philips Res. Rep. 9 (1954) 295–365.
[19] A. Malecki, J.A.K. Tareen, J.P. Doumerc, L. Rabardel, J.C. Launay, J. Solid State Chem. 56 (1985) 49–57.
[20] E. Aukrust, A. Muan, Trans. Met. Soc. AIME 230 (1964) 378–382.
[21] F.C.M. Driessens, Inorg. Chim. Acta 1 (1967) 193–201.
[22] K.S. Irani, A.P.B. Sinha, A.B. Biswas, J. Phys. Chem. Solids 23 (1962) 711–727.
[23] R.D. Shannon, Acta Cryst. A 32 (1976) 751–767.
[24] P. Poix, Bull. Soc. Chim. France 5 (1965) 1085–1087.
[25] P. Poix, C.R. Acad. Sci. Paris 268 (1969) 1139–1140.
[26] B. Boucher, R. Buhl, M. Perrin, J. Appl. Phys. 42 (1971) 1615–1617.
[27] S.E. Dorris, T.O. Masson, J. Am. Ceram. Soc. 71 (1988) 379–385.
[28] J.A.K. Tareen, A. Malecki, J.P. Doumerc, J.C. Launay, P. Dordor, M. Pouchard, P. Hagenmuller, Mater. Res. Bull. 19 (1984) 989–997.
[29] E.J.W. Verwey, Semiconducting Materials, Butterworths, Scientific Publications, London, 1951.
[30] B. Gillot, M. Kharroubi, R. Metz, R. Legros, A. Rousset, Solid State Ionics 44 (1991) 275–280.
[31] J.L. Martin de Vidales, P. Garcia-Chain, R.M. Rojas, E. Vila, O. Garcia-Martinez, J. Mater. Sci. 33 (1998) 1491–1496.
[32] M. Beley, L. Padel, J.C. Bernier, Ann. Chim. France 3 (1978) 429–452.